Metronidazole Lacks Activity against *Mycobacterium tuberculosis* in an In Vivo Hypoxic Granuloma Model of Latency

Lee G. Klinkenberg,[1] Lesley A. Sutherland,[1] William R. Bishai,[1,2] and Petros C. Karakousis[1,2]

[1]Center for Tuberculosis Research, Department of Medicine, Johns Hopkins University School of Medicine, and [2]Department of International Health, Johns Hopkins Bloomberg School of Public Health, Baltimore, Maryland

During human latent tuberculosis (TB) infection, dormant bacilli putatively reside within the hypoxic environment of caseating lung granulomas. The anaerobic drug metronidazole has antituberculous activity under hypoxic conditions in vitro but lacks activity against murine TB. In the present study, we used the hypoxia marker pimonidazole to demonstrate the presence of hypoxia in a novel in vivo granuloma model of *Mycobacterium tuberculosis* latency. We also used a high-throughput, microarray-based technique to identify mycobacterial genes essential to hypoxia and showed that this in vivo model correctly identified 51% of hypoxia-attenuated mutants, a significantly larger percentage than that identified by the mouse (29%) and guinea pig (29%) aerosol models of TB. Although isoniazid showed activity during the first 28 days of therapy and rifampin was active against dormant bacilli after the establishment of hypoxia, metronidazole showed no antituberculous activity in this in vivo hypoxic granuloma model of *M. tuberculosis* dormancy.

Latent tuberculosis (TB) infection (LTBI) poses a major obstacle to TB eradication [1, 2]. Human LTBI is characterized by tuberculin test positivity without clinical or radiographic findings [3]. LTBI apparently comprises a paucibacillary population of dormant organisms with reduced replication and metabolism [4] within host granulomas [5].

Hypoxia may be a primary microenvironmental condition responsible for *Mycobacterium tuberculosis* dormancy within granulomas associated with human LTBI [6]. Unlike LTBI, most active TB infections occur in well-oxygenated body sites [6], and cavities open to airways generally harbor greater bacillary numbers [7]. Furthermore, disease reactivation usually involves the highly oxygenated upper lung lobes [6].

Exposure of *M. tuberculosis* to progressive hypoxia in vitro induces a dormant state characterized by reduced replication and metabolism analogous to that postulated for bacilli in human LTBI. In the best-characterized model, Wayne and Hayes [8] and Wayne [9] have shown that, when the dissolved oxygen content drops below 1%, *M. tuberculosis* enters microaerophilic nonreplicating persistence (NRP) stage 1 [8], which is characterized by termination of DNA synthesis and thickening of the outer cell wall. As the dissolved oxygen content drops to ~0.06%, the bacilli enter NRP stage 2 and demonstrate reduced susceptibility to standard antituberculous drugs but increased susceptibility to nitroimidazole drugs [8, 10].

Metronidazole becomes reductively activated by the pyruvate-ferredoxin oxidereductase system under anoxic conditions [11]. Despite activity against dormant bacilli under progressive-hypoxia conditions in vitro, metronidazole appears to be inactive against *M. tuberculosis* in vivo. Specifically, metronidazole lacks activity against bacilli within infected bone marrow–derived macrophages and does not kill bacilli in mouse lungs

Received 13 December 2007; accepted 8 February 2008; electronically published 19 May 2008.

Potential conflicts of interest: none reported.

Presented in part: 46th Interscience Conference on Antimicrobial Agents and Chemotherapy, San Francisco, 27–30 September 2006 (poster B-1321); Keystone Symposia: Tuberculosis: From Lab Research to Field Trials, Vancouver, 20–25 March 2007 (posters 260 and 267); 45th annual meeting of the Infectious Diseases Society of America, San Diego, 4–7 October 2007 (poster 343).

Financial support: National Institutes of Health (grants AI043846, AI37856, AI36973, and AI007608 and contract AI30036 to W.R.B., and grant AI064229 to P.C.K.); Potts Memorial Foundation (fellowship to L.G.K.).

Reprints or correspondence: Dr. Petros Karakousis, Center for Tuberculosis Research, Johns Hopkins University School of Medicine, 1550 Orleans St., Rm. 110, Baltimore, MD 21231-1001 (petros@jhmi.edu).

The Journal of Infectious Diseases 2008; 198:275–83

0022-1899/2008/19802-0018$15.00
DOI: 10.1086/589515

Table 1. *Himar1* transposon mutants included in pool 1.

The table is available in its entirety in the online edition of the *Journal of Infectious Diseases*.

during the active or containment phases of disease [12]. Furthermore, metronidazole lacks sterilizing activity in the Cornell model of murine TB persistence [12, 13]. However, the poor antituberculous activity of metronidazole in the mouse model may be explained by the absence of hypoxia in mouse lungs during TB infection [14, 15].

We developed a novel in vivo granuloma model of *M. tuberculosis* dormancy (the mouse hollow-fiber model) in which bacilli achieve stationary-state colony-forming unit counts, decreased metabolic activity, and greater susceptibility to rifampin than isoniazid, which are key features of human LTBI [16]. In this model, host inflammatory cells are recruited around the subcutaneously implanted semidiffusible fibers, resulting in progressive formation of perifiber granulomas. Dormant organisms in this model show significant up-regulation of the DosR regulon, which is also induced on hypoxic exposure of bacilli in vitro [17].

In the present study, we characterized the oxygen content in the mouse hollow-fiber model by means of the hypoxia marker pimonidazole as well as a high-throughput microarray-based technique to evaluate the survival of several different *M. tuberculosis* mutants containing mutations in hypoxia-induced genes. Having found evidence of hypoxia using these immunohistochemical and mutant-survival approaches, we tested the tuberculocidal activity of metronidazole in the mouse hollow-fiber model.

METHODS

Strain selection criteria. Insertion mutagenesis of *M. tuberculosis* CDC1551 by means of the *Himar1* transposon (Tn) yielded a library of ~1500 unique mutants [18]. Tn insertion sites were identified by sequencing [18, 19]. Available mutants were cross-referenced with a list of hypoxia-induced genes compiled from published data [20–24], and 107 mutants were selected for this study (tables 1 and 2).

Bacterial strains and growth conditions. Tn mutants were grown individually to mid-log phase at 37°C in Middlebrook 7H9 liquid broth supplemented with oleic acid–albumin–dextrose–catalase (Becton Dickinson), 0.05% Tween-80, and 0.1% glycerol. Equal volumes of same-density cultures were mixed, forming 2 pools (tables 1 and 2). Glycerol was added to a final concentration of 10%, and aliquots (optical density [OD] at 600 nm, 0.4) were frozen at −80°C.

Progressive-hypoxia model of infection. Each Tn mutant pool culture was diluted to ~1×10^4 cfu/mL, as determined by OD_{600}. A culture with a ratio of head-space air to medium volume of 0.5 was grown in individual test tubes containing a magnetic stir bar and sealed with rubber stoppers. The cultures were incubated upright at 37°C with stir bars spun at a speed sufficient for uniform suspension of organisms without agitating the culture surface. The reduction and decolorization of the methylene blue dye served as a visual indicator of oxygen levels corresponding to NRP stage 2 [8], and the day on which this occurred was defined as day 0. Samples were collected on day 0 (input pool) and on day 28 (output pool) after color change. Sample collection, done by piercing the rubber stoppers, did not introduce atmospheric oxygen into the tubes, as assessed by maintenance of the decolorized dye state.

Animals. Female SKH1 hairless immunocompetent mice (7–8 weeks old) and female outbred Hartley guinea pigs (300–350 g) were purchased from Charles River Laboratories. Animals were maintained under pathogen-free conditions and were fed water and chow ad libitum. All procedures followed protocols approved by the Institutional Animal Care and Use Committee of the Johns Hopkins University.

Aerosol infection of animals. Animals were aerosol infected with the pools of Tn mutants by means of a Glas-Col inhalation exposure system, calibrated to deliver ~500 cfu/lung on day 1 after infection. Animals were killed on day 14 (input pool) and on day 56 (output pool), and organs were removed aseptically. Day 14 was chosen as the input time point to allow for adequate representation of each individual Tn mutant before organized granuloma formation in animal lungs. Guinea pig organs were stored at -80 °C until the time of homogenization. Guinea pig lungs were homogenized in 5–10 mL of PBS by means of a Polytron homogenizer (Kinematica) with a 12-mm generator (Brinkman) in a biosaftey level 3 Glovebox cabinet (Germfree). Mouse lungs were homogenized using glass homogenizers.

Hollow-fiber infection of mice. Approximately 1×10^4 organisms of 2 separate Tn mutant pools from the same mixed culture as the aerosol infections were inoculated into each individual hollow fiber (~200 cfu per mutant). Fibers were heat sealed and implanted subcutaneously, as described elsewhere [16, 25, 26]. Mice were killed and fibers recovered on day 14 (input pool) and on day 56 (output pool) after fiber implantation.

Mutant pool recovery and genomic preparations. Samples were plated on supplemented Middlebrook 7H10 plates (Fisher). Log_{10}-transformed colony-forming unit counts were used to calculate averages and SDs for graphing purposes. From 500 to 10,000 colonies per sample (as available) were scraped from plates and pooled, and genomic DNA was extracted as described

Table 2. *Himar1* transposon mutants included in pool 2.

The table is available in its entirety in the online edition of the *Journal of Infectious Diseases*.

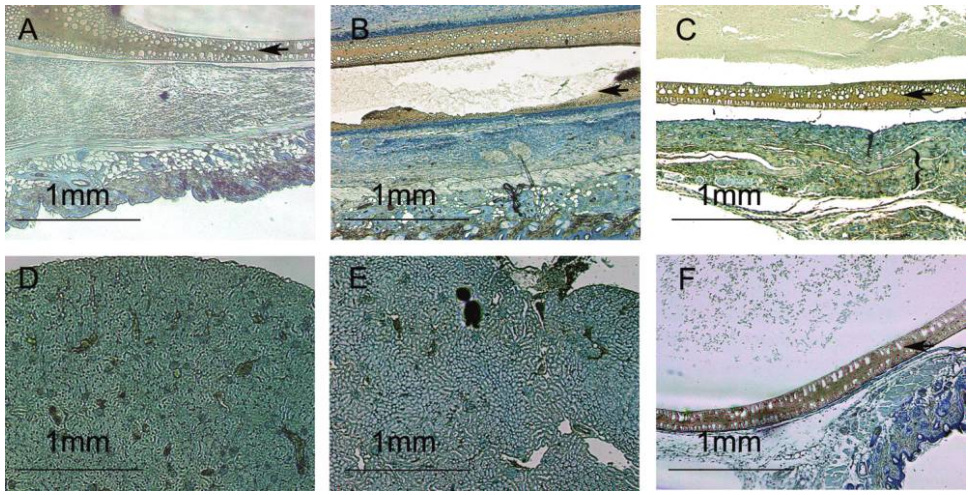

Figure 1. Pimonidazole staining of perifiber tissues. Hollow fibers were recovered on days 7 *(A),* 14 *(B),* and 28 *(C)* after implantation. Also shown are positive controls comprising cross-sections of mouse kidney on days 7 *(D)* and 14 *(E)* after fiber implantation and hollow fiber containing vehicle recovered on day 28 after implantation *(F).* Arrows indicate hollow fiber wall. The bracket in panel C shows the layer of greatest inflammation and pimonidazole staining.

elsewhere [27]. DNA samples were processed according to the DeADMAn (designer arrays for defined mutant analysis) technique [28]. Samples generated from input and output pools for each experiment were labeled with different fluorochromes, combined, and hybridized to mutant-specific 60mer microarrays. Control probes were printed onto the array as a mix of all 107 mutant-specific 60mers and used to normalize the ratio of signal between the 2 channels. The variance of each ratio between at least 2 technical replicates of 2 biological replicates was analyzed using SAM software (version 3.01) [29]. Probes with greater signal from the input pool than from the output pool were determined to reflect attenuation of a particular Tn mutant if the corresponding *q* value was less than the false discovery rate, selected such that the mean number of false discoveries was <1 gene per array.

Metronidazole chemotherapy. Hollow fibers containing ~1000 *M. tuberculosis* CDC1551 bacilli were implanted into SKH1 mice. Antibiotic therapy was initiated 14 days after implantation. Groups of mice were treated daily (5 days per week) by esophageal cannulation (gavage) with isoniazid (25 mg/kg/day), rifampin (10 mg/kg/day), metronidazole (100 mg/kg/day), or pyrazinamide (150 mg/kg/day). A control group received deionized water daily by gavage. Mice were killed and hollow fibers retrieved on days −13, −7, 0, 7, 14, 28, and 56 relative to initiation of treatment. Hollow-fiber contents were plated on 7H10 plates, and bacterial colonies

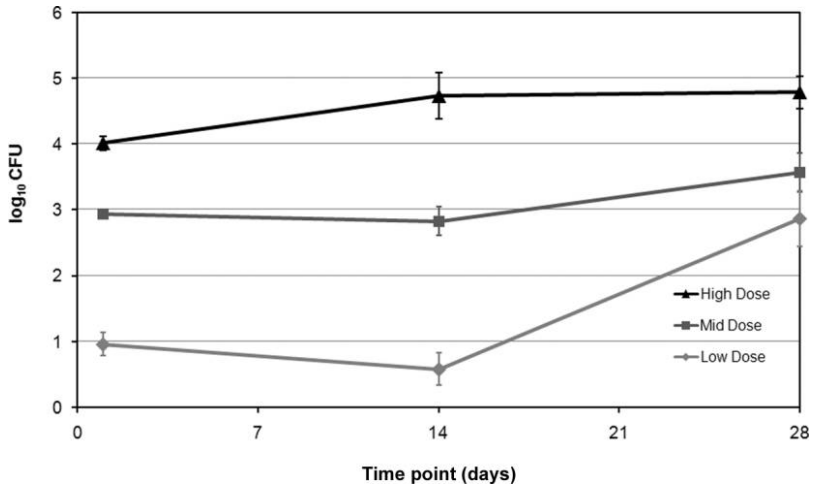

Figure 2. Colony-forming unit counts from hollow fibers used for pimonidazole immunohistochemical analysis. Separate groups of mice received hollow fibers containing ~10 cfu (low dose), ~1×10^3 cfu (mid-dose), and ~3.5×10^4 cfu (high dose). Values are $\log_{10}$-transformed colony-forming unit counts with SDs. Results of pimonidazole staining for these experiments are presented in figure 3.

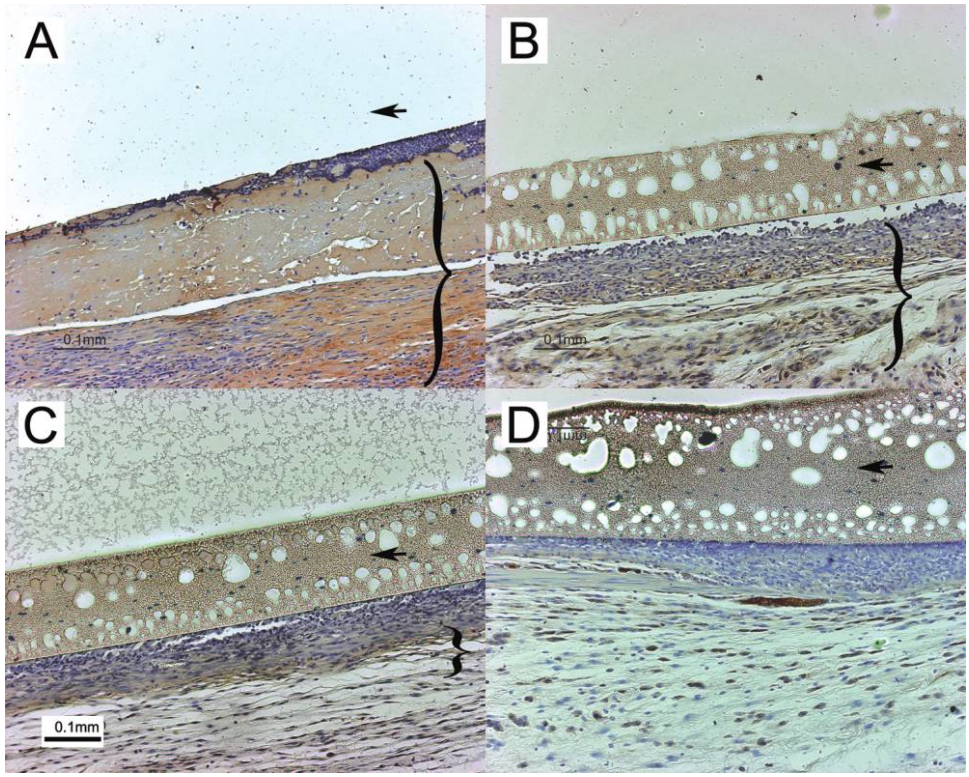

Figure 3. Dependence of perifiber hypoxia on the no. of intrafiber bacilli. Shown are cross-sections of hollow fibers containing a low dose *(A),* mid-dose *(B),* or high dose *(C)* of colony-forming units or ~3.5×10^4 heat-killed organisms *(D).* The arrow in panel A indicates the location of missing hollow-fiber wall. The arrows in panels B–D indicate hollow-fiber walls. The brackets in panels A–C indicate tissue layers containing pimonidazole staining.

were enumerated after 3 weeks. Results are representative of 2 independent experiments.

Pimonidazole immunohistochemical analysis. Fibers containing ~3000 cfu of bacilli were implanted into one group of 20 SKH1 mice, and groups of 5 animals were killed on days 1, 7, 14, and 28 after implantation. Three additional groups of 15 mice received fibers containing ~10, ~1×10^3, or ~1×10^4 cfu, and 5 mice from each group were killed on days 1, 14, and 28 after implantation. Mice received pimonidazole (Chemicon International; 60 mg/kg by intraperitoneal injection) 2 h before being killed. Hollow-fiber contents from 3 mice per time point were used for colony-forming unit enumeration. The remaining hollow fibers were removed in situ and placed in 10% neutral buffered formalin. Paraffin-embedded tissue sections were visualized for pimonidazole staining according to manufacturer recommendations.

Table 3. ***Himar1*** **transposon mutant survival in 4 models, including the in vitro progressive-hypoxia model (reference).**

Pool, model	Mutants attenuated in each model, total no.	Hypoxia-attenuated mutants in each model, proportion (%)
Pool 1		
Hypoxia reference model	21	21/21 (100)
Mouse hollow-fiber model	43	14/21 (67)
Mouse aerosol model	14	6/21 (29)
GP aerosol model	10	6/21 (29)
Pools 1 and 2		
Hypoxia reference model	74	74/74 (100)
Mouse hollow-fiber model	67	38/74 (51)

RESULTS

Perifiber tissue staining with the hypoxia marker pimonidazole. To test directly for the presence of microaerophilic conditions in the mouse hollow-fiber model, we used the hypoxia marker pimonidazole. This 2-nitroimidazole becomes activated by mammalian nitroreductases and stably binds to cellular proteins at tissue pO_2 levels <10 mm Hg [30]. This binding can be detected in tissue sections by immunostaining with a monoclonal antibody to pimonidazole adducts. Tissue pimonidazole adducts yield chromogenic production of a brown color through a horseradish peroxidase–linked reaction. Interestingly, the hollow-fiber walls appeared brown in all samples, even in the absence of primary antibody.

In a preliminary experiment, ~1×10^3 bacilli were encapsulated and implanted subcutaneously in mice. Although pi-

Table 4. Survival of individual *Himar1* transposon mutants in the hypoxia reference model.

MT	Rv	Name	Models attenuated[a]	Fold attenuation[b]
MT0023	Rv0020c	*TB39.8*	R, Mo HF, Mo Aero	10.64
MT0595	Rv0569	. . .	R, Mo HF, Mo Aero	2.30
MT0607	Rv0578c	*PE_PGRS7*	R	1.87
MT0845	Rv0823c	. . .	R, Mo HF	2.07
MT0909	Rv0886	*fprB*	R, Mo HF, Mo Aero	3.57
MT1161	Rv1129c	. . .	R, Mo HF	2.00
MT1283	Rv1245c	. . .	R, Mo HF	2.56
MT1449	Rv1405c	. . .	R	<1.00
MT1944	Rv1894c	. . .	R, Mo HF, GP Aero	36.92
MT2084	Rv2025c	. . .	R, GP HF, GP Aero	<1.00
MT2090	Rv2031c	*hspX/acr*	R, Mo HF	8.30
MT2137	Rv2077c	. . .	R, Mo HF, GP Aero	4.25
MT2940	Rv2873	*mpt83*	R, Mo Aero, GP Aero	3.06
MT3220	Rv3134c	. . .	R, Mo HF	150.73
MT3851	Rv3743c	*ctpJ*	R, Mo Aero	1.19

NOTE. GP Aero, guinea pig aerosol model; HF, mouse hollow-fiber model; Mo Aero, mouse aerosol model; R, in vitro progressive-hypoxia model (reference).

[a] Models in which each particular mutant was found to be attenuated by DeADMAn (designer arrays for defined mutant analysis; see Methods for details).

[b] Values represent fold attenuation in the reference model at 28 days relative to day 0, determined by enumeration of colony-forming units for individually grown mutant strains.

monidazole adducts were undetectable on day 7 or 14 after fiber implantation (figure 1*A* and 1*B*), perifiber staining was observed on day 28 in fibers containing live bacilli (figure 1*C*) but not in those containing vehicle (figure 1*F*). Negative in situ fiber staining results are accompanied by corresponding positively staining kidney sections (figure 1*D* and 1*E*) containing hypoxic renal tubular cells [31].

To determine whether hypoxia in the mouse hollow-fiber model is a dose-dependent phenomenon, hollow fibers containing ~10 cfu (low dose), $\sim 1 \times 10^3$ cfu (mid-dose), or $\sim 1 \times 3.5 \times 10^4$ cfu (high dose) were implanted subcutaneously into separate groups of mice. Control mice received fibers containing $\sim 3.5 \times 10^4$ heat-killed bacilli. As shown in figure 2, the total number of colony-forming units increased <10-fold over a 28-day period (for high dose, $P = .03$; for mid-dose, $P = .09$) except in the low-dose group, where the intrafiber colony-forming unit count reached $\sim 1 \times 10^3$ by day 28 after fiber implantation ($P < .002$). The degree of perifiber cellular inflammation and pimonidazole staining intensity on day 28 appeared to directly correlate with the number of encapsulated live bacilli on day 1 (figure 3).

M. tuberculosis *genes required for survival during hypoxia and in animal models.* Genomewide expression analysis using microarrays provides a powerful means to study adaptive bacterial survival strategies in response to various stress conditions [32]. *M. tuberculosis* gene regulation during hypoxia has been monitored in vitro [20–24], revealing induction of genes potentially involved in bacillary survival under these conditions. We hypothesized that *M. tuberculosis* genes induced during hypoxia may be important for mycobacterial hypoxic survival.

We screened an archived library of ~1500 unique *M. tuberculosis* CDC1551 Tn insertion mutants [18] for mutations in hypoxia-induced genes [20–24] and selected a total of 107 different mutants, which were split into 2 pools (tables 1 and 2). These mutants were tested for survival in a reference model of progressive hypoxia in vitro [8], using a high-throughput microarray-based approach termed DeADMAn [28]. These mutants also were tested for survival in the mouse hollow-fiber model, and a subset of mutants were tested in the mouse and guinea pig aerosol models of infection. Mutant survival patterns in each model were compared with those in the reference model.

Of the 107 mutants tested in the reference model, 74 were significantly attenuated (mean false-positive results per array <1) relative to the wild-type strain by day 28 after entry of the organisms into NRP stage 2 (table 3). Fifteen of the 74 mutant strains were grown individually in this model to confirm the microarray survival data from the pooled groups. Thirteen of these 15 Tn mutants showed reduced colony-forming unit counts relative to that of the isogenic wild-type strain by day 28 after entry into NRP stage 2 (table 4). Of these 13 mutants, 11 were attenuated by 2-fold or more and 3 mutants (containing Tn insertions in Rv3134c, Rv1894c, and Rv0020c) were attenuated by at least 10-fold relative to the wild-type strain.

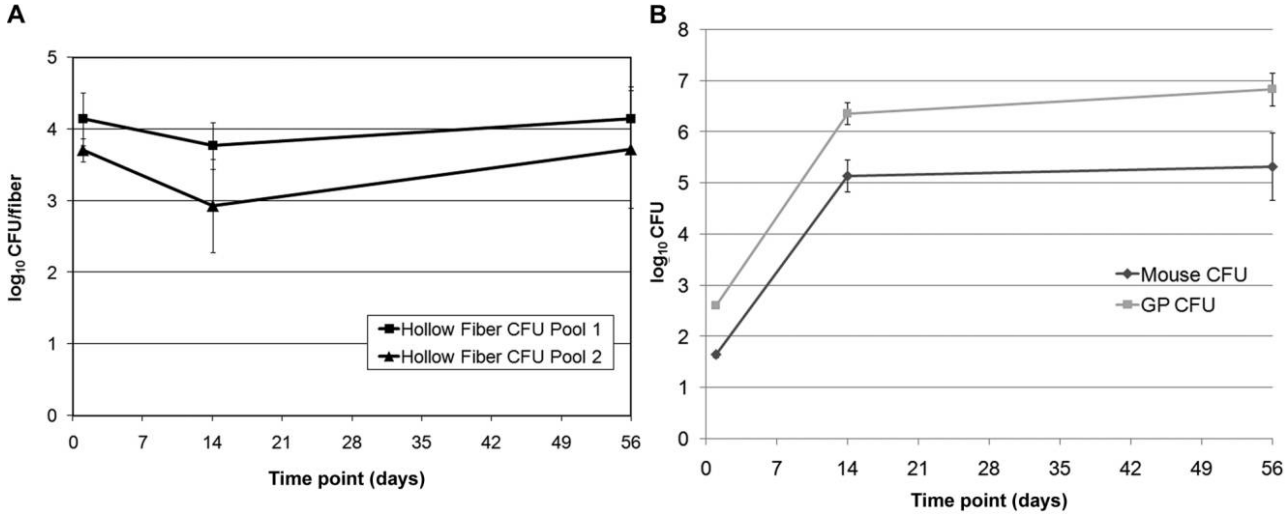

Figure 4. Total mutant colony-forming unit counts in hollow fibers *(A)* and in guinea pig and mouse lungs *(B)* as a function of time. Colony-forming unit counts were $\log_{10}$ transformed; error bars show SDs.

The 2 Tn mutant pools (tables 1 and 2) were next tested in the mouse hollow-fiber model. Total intrafiber colony-forming unit counts for both mutant pool 1 and 2 remained stable between days 14 and 56 after hollow-fiber implantation (for pool 1, $P = .14$; for pool 2, $P = .18$) (figure 4*A*). Of the 21 attenuated mutants in the reference model, 14 (67%) were attenuated relative to the wild-type strain by day 56 in the mouse hollow-fiber model (table 3). Of the 74 total mutants found to be defective for survival in the reference model, 38 (51%) also were attenuated relative to the wild-type strain by day 56 in the mouse hollow-fiber model (table 3). An additional 29 mutants among both pools showed reduced survival compared with the wild-type strain by day 56 in the mouse hollow-fiber model but not in the reference model, presumably reflecting conditions present in the former model but absent in the latter.

Recent studies have reported hypoxia in guinea pig tuberculous lung lesions [33] but not in mouse lung lesions [14, 15]. We hypothesized that Tn mutants containing mutations in genes required for microaerophilic survival of *M. tuberculosis* would show an attenuated phenotype in guinea pig lungs but not in mouse lungs. Guinea pigs and mice were infected with Tn mutant pool 1 by aerosol, and lung samples were collected for colony-forming unit enumeration (figure 4*B*) and mutant survival analysis. Between days 14 and 56, colony-forming unit counts in mouse lungs remained relatively stable ($P = .64$), whereas colony-forming unit counts in guinea pig lungs increased slightly ($P < .05$), consistent with bacillary growth containment after the onset of adaptive immunity [34]. Of the 21 Tn mutants found to be attenuated in the reference model, 4 (19%) were attenuated in guinea pig lungs relative to the wild-type strain by day 56 after infection. Six (29%) of the 21 hypoxia-attenuated mutants showed reduced survival in mouse lungs relative to the wild-type strain by day 56 after infection (table 3). Only the mutant containing a Tn insertion in Rv2873, which encodes the highly immunogenic cell-surface lipoprotein mpt83 [35], was attenuated in both mouse and guinea pig lungs.

A mutant with a Tn insertion in the *narG* gene, the product of which is involved in the alternate respiration nitrate-reduction pathway, was attenuated only in the mouse hollow-fiber model and not in the other models tested. Mutants with Tn insertions in Rv2031c, which encodes HspX (α-crystallin), and in Rv3134c, the gene immediately upstream of *dosR/devR,* were attenuated only in the reference and mouse hollow-fiber models and not in the mouse or guinea pig aerosol models.

Metronidazole activity in the mouse hollow-fiber model. On exposure to progressive hypoxia in vitro, *M. tuberculosis* becomes phenotypically tolerant to the first-line antituberculous agents isoniazid and rifampin and increasingly susceptible to metronidazole [8, 10]. Given the positive tissue-staining results with pimonidazole in the mouse hollow-fiber model as well as the relatively high number of hypoxia-attenuated Tn mutants identified in this model compared with the mouse aerosol model, we next tested the activity of metronidazole against *M. tuberculosis* in the mouse hollow-fiber model. Beginning 14 days after fiber implantation, mice received therapy 5 days per week with isoniazid (25 mg/kg), rifampin (10 mg/kg), pyrazinamide (150 mg/kg), or metronidazole (100 mg/kg), and control mice received vehicle by gavage. As demonstrated in figure 5, metronidazole had no significant activity against bacilli during the first 56 days after infection. Isoniazid had the greatest bactericidal activity during the first 28 days after fiber implantation ($P < .01$), with no activity thereafter ($P = .47$). Conversely, rifampin showed minimal activity during the first 28 days ($P = .7$) but reduced intrafiber colony-forming unit counts by 2 $\log_{10}$ by day 56 after implantation ($P < .05$). Consistent with data from the standard mouse model [36], pyrazin-

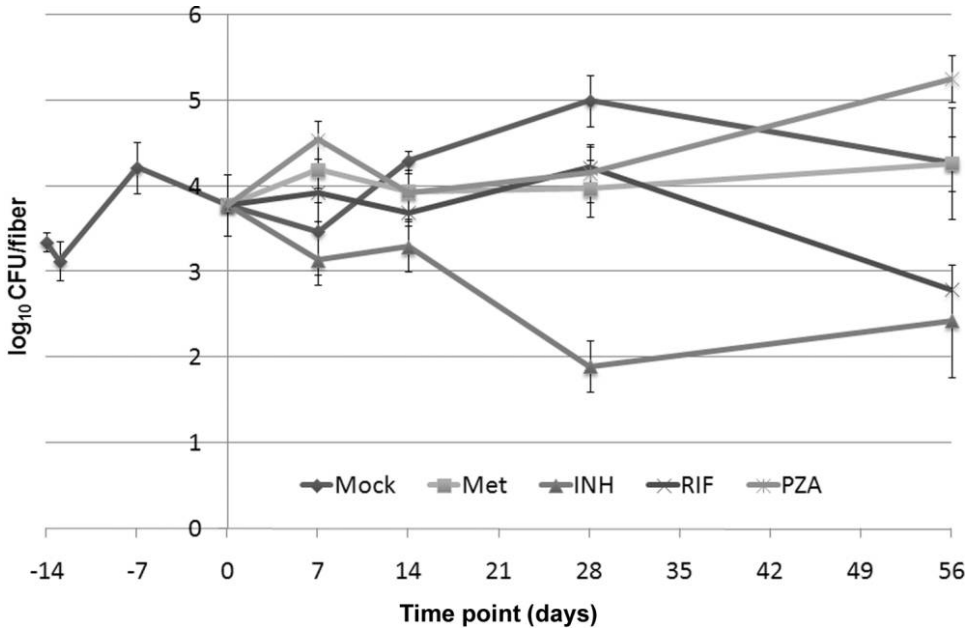

Figure 5. Activity of metronidazole against bacilli in the mouse hollow-fiber model. Mice were either mock treated (Mock) or treated with metronidazole (Met) at 100 mg/kg/day, isoniazid (INH) at 25 mg/kg/day, rifampin (RIF) at 10 mg/kg/day, or pyrazinamide (PZA) at 150 mg/kg/day by esophageal cannulation beginning 14 days after hollow-fiber implantation. Colony-forming unit counts were $\log_{10}$ transformed; error bars show SDs.

amide alone had no bactericidal activity against hollow fiber–encapsulated *M. tuberculosis*.

DISCUSSION

Exposure of *M. tuberculosis* to progressive hypoxia induces a nonreplicating persistent state characterized by reduced susceptibility to isoniazid and rifampin, which is analogous to human LTBI. However, this in vitro model has been criticized because the organisms become susceptible to metronidazole, yet this antibiotic lacks tuberculocidal activity in the murine model [12, 13]. Data are lacking to support its activity against human LTBI. In addition, in vitro models cannot accurately simulate the complex host-pathogen interactions involved in bacillary containment during human LTBI. We have developed a novel in vivo granuloma model of LTBI (the mouse hollow-fiber model) in which bacillary growth containment is partially immune mediated and the organisms exhibit a dormancy phenotype characteristic of human LTBI [16]. Consistent with the presence of microaerophilic conditions in this model, the organisms show significant up-regulation of the DosR regulon. We used the hypoxia-specific marker pimonidazole to directly demonstrate reduced tissue oxygen content in this in vivo model. The findings of *M. tuberculosis* dose-dependent pimonidazole staining as well as the absence of cellular inflammation and pimonidazole staining surrounding fibers containing heat-killed bacilli are consistent with active secretion and extrafiber diffusion of *M. tuberculosis* soluble factors leading to host inflammatory cell recruitment, perifiber granuloma formation, and ensuing hypoxia. Consistent with previous data [37], our data suggest a role for hypoxia in promoting *M. tuberculosis* dormancy beyond day 28 in this model, after which time the organisms become phenotypically resistant to isoniazid but susceptible to rifampin.

To our knowledge, this is the first study in which the accuracy of stress-induced *M. tuberculosis* gene expression in predicting gene function was tested systematically on a large scale. We investigated the role played by various hypoxia-induced genes in mycobacterial survival under microaerophilic conditions thought to be present in human caseous TB lesions. Identification of *M. tuberculosis* genes essential for hypoxic survival potentially provides a basis for rational drug design targeting dormant organisms in human LTBI. Approximately 69% (74/107) of all hypoxia-induced genes were found to be essential for survival during progressive hypoxia. This percentage is significantly higher than that observed using random Tn mutant pools under various stress conditions (25%–30%; authors' unpublished data), consistent with our original hypothesis that mycobacterial gene induction predicts gene essentiality under the same stress conditions.

Among the *M. tuberculosis* genes identified as being essential for bacillary survival during hypoxia were Rv3134c, Rv0823c, Rv1129, Rv1894c, and Rv0020c. Rv3134c is directly upstream of both genes of the 2-component response regulator, *dosR/dosS,* raising the possibility that its disruption might have polar effects on genes downstream of this operon, which is required for *M. bovis* survival under hypoxic conditions [38]. The genes Rv0823c and Rv1129c encode putative transcriptional regulators that

may be involved in DosR-independent hypoxic gene regulation. The Rv0020c-encoded protein is predicted to have a forkhead-associated domain, which is a phosphopeptide-binding motif and putative nuclear signaling domain present in many regulatory proteins. The conserved hypothetical protein encoded by Rv1894c has weak similarity to some oxidoreductases. Additionally, each Tn mutant tested that contained an interruption of a member of the DosR regulon (Rv0079, Rv0081, Rv0569, Rv1736c, Rv2029c, Rv2031c, Rv2626c, and Rv3134c) was attenuated during hypoxia, further corroborating the importance of the DosR regulon in the adaptation of *M. tuberculosis* to hypoxia.

Consistent with greater hypoxia in the mouse hollow-fiber model, more hypoxia-attenuated mutants were detected in this model relative to the mouse and guinea pig aerosol models. Surprisingly, the guinea pig model was not superior to the standard mouse model in detecting such mutants. One explanation is potential variability in pathology and tissue microenvironments throughout guinea pig lungs, such that distinct bacillary populations experience different oxygen tensions. Another possibility is that granuloma caseation was not complete at the output sample time points selected and that more hypoxia-attenuated mutants would be detected at later time points.

The findings of metronidazole inactivity in the murine model of TB [12, 13] have been criticized by proponents of the antituberculous activity of the drug, because mouse TB lesions do not achieve the degree of hypoxia necessary for drug activation [14, 15]. Here, we report no antituberculous activity of metronidazole in a novel in vivo granuloma model of *M. tuberculosis* dormancy, despite immunohistochemical and mutant survival–based evidence of hypoxia. There are several potential explanations for our results. Because intrafiber metronidazole concentrations were not directly measured, it is possible that intrafiber bacilli received suboptimal drug exposure. In this study, isoniazid and rifampin showed activity against intrafiber bacilli, suggesting bioavailability of these drugs following gavage. The oral metronidazole dose we used (100 mg/kg) equals or exceeds that used in previous murine TB studies [12, 13] and is greater than that shown to have activity against *Bacteroides fragilis* and *Neisseria gonorrhoeae* [39, 40] subcutaneous abscesses in mice, suggesting bioavailability of the drug in the subcutaneous space after oral administration. Alternatively, metronidazole may have poor penetration into granulomatous lesions. In that case, however, the drug would be expected to have minimal activity against persistent bacilli in human TB infection, because these organisms are postulated to inhabit the caseous and necrotic cores of granulomas. Finally, tissue oxygen levels in the mouse hollow-fiber model may be microaerophilic but not sufficiently hypoxic to permit reductive activation of metronidazole.

It remains to be conclusively demonstrated whether persistent bacilli in human TB infection dwell in caseous and necrotic lesions and whether these lesions are sufficiently hypoxic to permit metronidazole activation. Ultimately, the utility of metronidazole as an antituberculous drug can only be addressed directly in a prospective, randomized clinical trial.

References

1. Dye C, Scheele S, Dolin P, Pathania V, Raviglione MC. Consensus statement. Global burden of tuberculosis: estimated incidence, prevalence, and mortality by country. WHO Global Surveillance and Monitoring Project. JAMA **1999**; 282:677–86.
2. Lillebaek T, Dirksen A, Baess I, Strunge B, Thomsen VO, Andersen AB. Molecular evidence of endogenous reactivation of *Mycobacterium tuberculosis* after 33 years of latent infection. J Infect Dis **2002**; 185:401–4.
3. Tufariello JM, Chan J, Flynn JL. Latent tuberculosis: mechanisms of host and bacillus that contribute to persistent infection. Lancet Infect Dis **2003**; 3:578–90.
4. Nuermberger E, Bishai WR, Grosset JH. Latent tuberculosis infection. Semin Respir Crit Care Med **2004**; 25:317–36.
5. Opie EL, Aronson JD. Tubercle bacilli in latent tuberculous lesions and in lung tissue without tuberculous lesions. Arch Pathol Lab Med **1927**; 4:1–21.
6. Adler JJ, Rose DN. Transmission and pathogenesis of tuberculosis. In: Rom WN, Garay SM, eds. Tuberculosis. 1st ed. Boston: Little, Brown & Company, **1996**:1002.
7. Canetti G. The tubercle bacillus in the pulmonary lesion of man: histobacteriology and its bearing on the therapy of pulmonary tuberculosis. American rev. ed. New York: Springer, **1955**.
8. Wayne LG, Hayes LG. An in vitro model for sequential study of shiftdown of *Mycobacterium tuberculosis* through two stages of nonreplicating persistence. Infect Immun **1996**; 64:2062–9.
9. Wayne LG. Synchronized replication of *Mycobacterium tuberculosis*. Infect Immun **1977**; 17:528–30.
10. Wayne LG, Sramek HA. Metronidazole is bactericidal to dormant cells of *Mycobacterium tuberculosis*. Antimicrob Agents Chemother **1994**; 38: 2054–8.
11. Edwards DI. Nitroimidazole drugs—action and resistance mechanisms. I. Mechanisms of action. J Antimicrob Chemother **1993**; 31:9–20.
12. Brooks JV, Furney SK, Orme IM. Metronidazole therapy in mice infected with tuberculosis. Antimicrob Agents Chemother **1999**; 43:1285–8.
13. Dhillon J, Allen BW, Hu YM, Coates AR, Mitchison DA. Metronidazole has no antibacterial effect in Cornell model murine tuberculosis. Int J Tuberc Lung Dis **1998**; 2:736–42.
14. Aly S, Wagner K, Keller C, et al. Oxygen status of lung granulomas in *Mycobacterium tuberculosis*-infected mice. J Pathol **2006**; 210:298–305.
15. Tsai MC, Chakravarty S, Zhu G, et al. Characterization of the tuberculous granuloma in murine and human lungs: cellular composition and relative tissue oxygen tension. Cell Microbiol **2006**; 8:218–32.
16. Karakousis PC, Yoshimatsu T, Lamichhane G, et al. Dormancy phenotype displayed by extracellular *Mycobacterium tuberculosis* within artificial granulomas in mice. J Exp Med **2004**; 200:647–57.
17. Voskuil MI, Schnappinger D, Visconti KC, et al. Inhibition of respiration by nitric oxide induces a *Mycobacterium tuberculosis* dormancy program. J Exp Med **2003**; 198:705–13.
18. Lamichhane G, Zignol M, Blades NJ, et al. A postgenomic method for predicting essential genes at subsaturation levels of mutagenesis: application to *Mycobacterium tuberculosis*. Proc Natl Acad Sci USA **2003**; 100: 7213–8.
19. Rubin EJ, Akerley BJ, Novik VN, Lampe DJ, Husson RN, Mekalanos JJ. In vivo transposition of mariner-based elements in enteric bacteria and mycobacteria. Proc Natl Acad Sci USA **1999**; 96:1645–50.
20. Muttucumaru DG, Roberts G, Hinds J, Stabler RA, Parish T. Gene expression profile of *Mycobacterium tuberculosis* in a non-replicating state. Tuberculosis (Edinb) **2004**; 84:239–46.

21. Park HD, Guinn KM, Harrell MI, et al. Rv3133c/dosR is a transcription factor that mediates the hypoxic response of *Mycobacterium tuberculosis*. Mol Microbiol **2003**; 48:833–43.
22. Sherman DR, Voskuil M, Schnappinger D, Liao R, Harrell MI, Schoolnik GK. Regulation of the *Mycobacterium tuberculosis* hypoxic response gene encoding alpha-crystallin. Proc Natl Acad Sci USA **2001**; 98:7534–9.
23. Voskuil MI, Visconti KC, Schoolnik GK. *Mycobacterium tuberculosis* gene expression during adaptation to stationary phase and low-oxygen dormancy. Tuberculosis (Edinb) **2004**; 84:218–27.
24. Rosenkrands I, Slayden RA, Crawford J, Aagaard C, Barry CE III, Andersen P. Hypoxic response of *Mycobacterium tuberculosis* studied by metabolic labeling and proteome analysis of cellular and extracellular proteins. J Bacteriol **2002**; 184:3485–91.
25. Hollingshead MG, Alley MC, Camalier RF, et al. In vivo cultivation of tumor cells in hollow fibers. Life Sci **1995**; 57:131–41.
26. Xu ZQ, Hollingshead MG, Borgel S, Elder C, Khilevich A, Flavin MT. In vivo anti-HIV activity of (+)-calanolide A in the hollow fiber mouse model. Bioorg Med Chem Lett **1999**; 9:133–8.
27. Ausubel FM. Current protocols in molecular biology. New York: Greene Pub. Associates and Wiley-Interscience: J Wiley, **1991**.
28. Lamichhane G, Tyagi S, Bishai WR. Designer arrays for defined mutant analysis to detect genes essential for survival of *Mycobacterium tuberculosis* in mouse lungs. Infect Immun **2005**; 73:2533–40.
29. Tusher VG, Tibshirani R, Chu G. Significance analysis of microarrays applied to the ionizing radiation response. Proc Natl Acad Sci USA **2001**; 98:5116–21.
30. Arteel GE, Thurman RG, Yates JM, Raleigh JA. Evidence that hypoxia markers detect oxygen gradients in liver: pimonidazole and retrograde perfusion of rat liver. Br J Cancer **1995**; 72:889–95.
31. MacManus MP, Maxwell AP, Abram WP, Bridges JM. The effect of hypobaric hypoxia on misonidazole binding in normal and tumour-bearing mice. Br J Cancer **1989**; 59:349–52.
32. Jenner RG, Young RA. Insights into host responses against pathogens from transcriptional profiling. Nat Rev Microbiol **2005**; 3:281–94.
33. Lenaerts AJ, Hoff D, Aly S, et al. Location of persisting mycobacteria in a Guinea pig model of tuberculosis revealed by r207910. Antimicrob Agents Chemother **2007**; 51:3338–45.
34. Mogues T, Goodrich ME, Ryan L, LaCourse R, North RJ. The relative importance of T cell subsets in immunity and immunopathology of airborne *Mycobacterium tuberculosis* infection in mice. J Exp Med **2001**; 193:271–80.
35. Hewinson RG, Michell SL, Russell WP, McAdam RA, Jacobs WR Jr. Molecular characterization of MPT83: a seroreactive antigen of *Mycobacterium tuberculosis* with homology to MPT70. Scand J Immunol **1996**; 43:490–9.
36. Lalande V, Truffot-Pernot C, Paccaly-Moulin A, Grosset J, Ji B. Powerful bactericidal activity of sparfloxacin (AT-4140) against *Mycobacterium tuberculosis* in mice. Antimicrob Agents Chemother **1993**; 37:407–13.
37. Karakousis PC, Williams EP, Bishai WR. Altered expression of isoniazid-regulated genes in drug-treated dormant *Mycobacterium tuberculosis*. J Antimicrob Chemother **2008**; 61:323–31.
38. Boon C, Dick T. *Mycobacterium bovis* BCG response regulator essential for hypoxic dormancy. J Bacteriol **2002**; 184:6760–7.
39. Brook I. Metronidazole and spiramycin therapy of mixed *Bacteroides* spp. and *Neisseria gonorrhoeae* infection in mice. Chemotherapy **1989**; 35:105–12.
40. Joiner KA, Lowe BR, Dzink JL, Bartlett JG. Antibiotic levels in infected and sterile subcutaneous abscesses in mice. J Infect Dis **1981**; 143:487–94.